PHILIPPINE ENGINEERING JOURNAL
PEJ 2020; Vol. 41, No. 2: 73-86

Pitting Corrosion of Steinmann Stainless Steel Pins in Simulated Body Fluid Using Cyclic Polarization Technique

Stephanie L. Santos and Manolo G. Mena
Department of Mining, Metallurgical and Materials Engineering, College of Engineering
University of the Philippines Diliman, Quezon City

Abstract *– Locally available Steinmann stainless steel pins were subjected to cyclic voltammetry in Kokubo simulated body fluid after immersion in SBF from 0 to 7 days. Results showed that the pins were susceptible to pitting corrosion from Day 0, with the degree of pitting increasing with the length of immersion. This may be due to the degradation of the initial passivation on the steel by SBF solution. SEM EDX analysis showed the presence of chloride precipitates in the pitting area. Chloride is known to induce autocatalytic corrosion of stainless steels. Optical Emission Spectroscopic analysis of the samples showed that one sample is SS304 and the other two were SS316L. The SS304 pins showed a higher tendency towards pitting corrosion when compared with the SS316L pins.*

Keywords – Steinmann pins, pitting corrosion, cyclic polarization

I. INTRODUCTION

Steinmann pins are one of the most common devices used in orthopaedic surgeries. It is a metallic rod with a trocar tip used for the initial fixation of fractured bones together. Steinmann pins are commonly made of surgical austenitic 316L stainless steel. Although well known for its biocompatibility, high mechanical strength and corrosion resistance, these materials still fail under severely corrosive environments such as human body fluid with high chloride concentration. As such, the suggested medical practice is to replace the 316L Steinmann pins with permanent implants such as Ti6Al4V alloys within two weeks.

When the implant is placed inside the human body, it is continuously exposed to extracellular tissue fluid and surface undergoes electrochemical dissolution releasing nickel, chromium and iron ions, powerful allergens and carcinogens resulting into sepsis in the tissues surrounding the implant. Pins retrieved from patients showed that corrosion due to pitting is the most common observable failure.

The contraction of sepsis and infection due to Steinmann pin corrosion is one of the problems in the orthopedic field in the Philippines. Commercially available pins are currently being sold without government inspection and quality control. The Philippine Orthopedic center alone inserted Steinmann pins into 1832 patients in 2015 [1]. The estimated usage worldwide is 1M orthopedic surgeries and expected to double by 2022 as the world's population and life expectancy increases [2]. This study will characterize locally available

Steinmann pins as to their composition and corrosion behaviour in simulated body fluid solution.

II. REVIEW OF RELATED WORK

2.1 Austenitic Stainless Steels

Austenitic stainless steel is a family of stainless steels containing at least 16% chromium and 6 % nickel, known for their toughness and ductility [3]. Nickel stabilizes the austenitic structure down to room temperature. Alloying elements such as molybdenum, titanium and copper are sometimes added for improved performance and high temperature and enhanced corrosion resistance.

Steinmann pins are commonly made from 316L stainless steels, which alloyed with molybdenum is a low carbon version of the 316 stainless steel. The lower carbon content precludes the formation of deleterious chromium carbide upon heat treatment, thus ensuring maximum corrosion resistance. Shown in Table 1 is the comparative compositions of 316 and 316L.

Table 1. Composition of 316 and 316L Stainless Steels [3]

Element	Type 316 (%)	Type 316L (%)
Carbon	0.08 max.	0.03 max.
Manganese	2.00 max.	2.00 max.
Phosphorus	0.045 max.	0.045 max.
Sulfur	0.03 max.	0.03 max.
Silicon	0.75 max.	0.75 max.
Chromium	16.00-18.00	16.00-18.00
Nickel	10.00-14.00	10.00-14.00
Molybdenum	2.00-3.00	2.00-3.00
Nitrogen	0.10 max.	0.10 max.
Iron	Balance	Balance

2.2 Simulated Body Fluids

Simulated body fluids (SBF) are solutions designed to mimic the ionic composition of blood plasma kept at mild conditions of pH and identical physiological temperature. The

solution was first introduced by Kokubo et al [4] in 1991 for their study of bioglass ceramics. Through the years, the solution has undergone various adjustments [5]. Shown in Table 2 is the composition of the Kokubo c-SBF (corrected SBF) as compared to human blood plasma. The SBF was subsequently used in the in vitro testing method to study the formation of apatite on the surface of bioimplants towards better bonding between bone and implant [5].

Table 2. Comparison of SBF and Blood Plasma Composition [5]

Ion	SBF	Blood Plasma
Na^+	142.0	142.0
K^+	5.0	5.0
Mg^{2+}	1.5	1.5
Ca^{2+}	2.5	2.5
Cl^-	148.8	103.0
HCO^{3-}	4.2	27.0
HPO_4^{2-}	1.0	1.0
SO_4^{2-}	0.5	0.5

2.3 Corrosion of Stainless Steels Implants

The in vivo corrosion of surgical grade stainless steel implants [2,5-7] is of great importance as the long-term degradation results in both loss in mechanical strength and infections due to ions released in the process. Chew reported that a four-year survey of stainless steel implants recovered from 50 patients in India showed that over 80% of the failures were due to severe localized corrosion attack such as pitting and crevice corrosion. Stress corrosion cracking that initiated from these pits and crevices were also observed. These failure mechanisms were also reported by Hansen [7]. As such, various enhancements in the metallurgy of stainless steels have been studied to improve its in vivo corrosion resistance. Yang [8] reported that the addition of 0.10% lanthanum in 316L stainless steel showed a widening of the passivation region and improvement in pitting corrosion resistance, most probably due to inclusion morphology modification and passive film formation. Chew observed that the addition of a hydrophoretically applied hydroxy apatite layer resulted in the formation of a protective insulating layer on the stainless steel surface [2].

2.4 Cyclic Polarization

Cyclic polarization is an electrochemical technique used to study the tendency of metals towards pitting corrosion. This technique investigates the onset of passivity, breakdown of the passive film, the susceptibility to repassivation. Cyclic polarization involves driving the test electrode anodically from the open cell potential until a large increase in current occurs and then reversing the scan direction until the loop closes. The size of the hysteresis loop area is taken as an indication of the susceptibility of the material towards pitting, with a larger

hysteresis loop area [9,10]. Such technique has been previously applied by Kamran [11] in the study of pitting resistance of SS316L in Ringer solution.

Figure 1 shows the typical cyclic polarization curve of a passivating metal. The rate of increase in the corrosion current is observed to decrease as the potential is driven anodically from the open cell corrosion potential, Ecorr to Epit, or pitting corrosion which is characterized by a sudden increase in the corrosion current. Upon reversing the direction of scan when the current reaches about 1 A/cm^2, a loop is created as the crosses the anodic scan line at Erep (also designated as Epro). Erep or Epro represents the protection potential of the metal due to the growth of a passivating film. The larger the area of the hysteresis loop, the higher is the tendency of the material to undergo pitting corrosion.

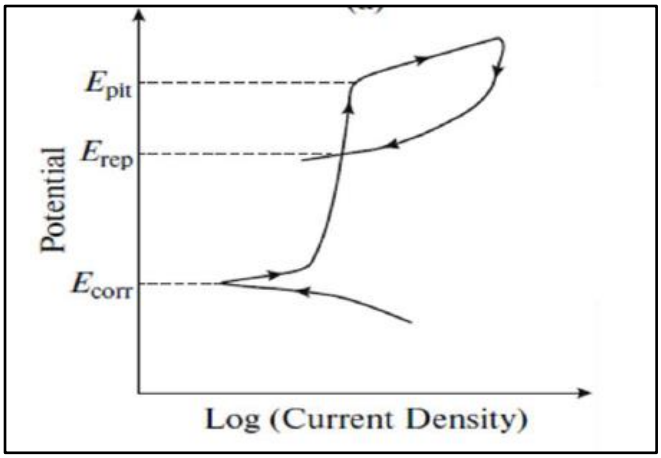

Figure 1. Cyclic Polarization Curve of a Passivating Metal [12]

III. METHODOLOGY

3.1 Materials and Equipment

In this study, three (3) commercially-available Steinmann pins were obtained from local suppliers. Sample A was reported by the vendor to have come from China. The origin of Samples B and Sample C were not identified. The pins had a diameter of 3.0 mm. Test specimen were cut from the samples using a Buehler Isomet Precision cutter. Chemical Analyses were performed on the test specimen using a XOS HDXRF x-ray fluorescence spectroscope (XRF) and SPECTROMAXx spark optical emission spectrometer (OES).

Test electrodes for the cyclic polarization testing were fabricated by soldering a lead copper wire to the specimen, and then encapsulating the electrode in epoxy. The exposed area subjected to sequential polishing from 120 to 1200 grit SiC abrasive paper and then down to 1 um polishing diamond in a Leco polisher. This surface preparation protocol was maintained throughout the study to eliminate surface roughness as a variable.

A three-electrode set up was used in this study, with the Steinmann pin as the working electrode, platinum as counter electrode and Ag/AgCl reference electrode a show in Figure 2.

The electrochemical cell was immersed in constant temperature water bath at 37 ^{o}C. The cyclic polarization test was conducted using a Metrohm Autolab PGSTAT 128N potentiometer. The potential of the working electrode was allowed to equilibrate at the open cell potential (OCP), which about 10 minutes before running the scan from minus 0.25 volt vs OCP to plus 0.25 volt vs OCP at the rate of 1 mV/s, until the potential reached 0.844 volt against the Ag/AgCl electrode. A Kokubo simulated fluid was used as electrolyte. The pH was kept constant at 7.4 using a tris(hydroxymethyl)aminomethane buffer solution. Figure 3 shows the electrochemical set up used in the experiments.

A Hitachi TM 4000 Scanning Electron Microscope (SEM) with a Bruker Nano Energy Dispersive Spectrometry (EDS) was used for surface characterization of the test specimen. EDS mapping was also performed on the pitted surfaces of the electrodes.

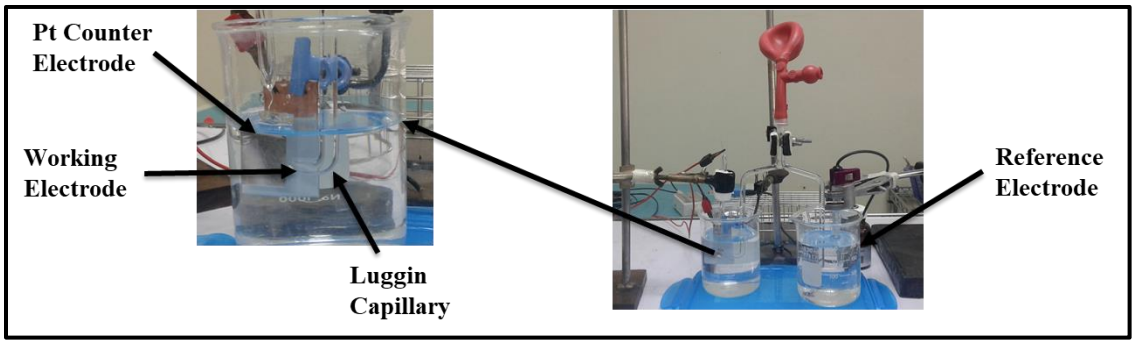

Figure 2. Three Electrode Cyclic Polarization Cell

3.2 Experimental Plan

Cyclic polarization tests were performed on samples that were soaked in the SBF at 0, 1, 3 and 7 days. The pitting potential, Epit and protection potential Epro were determined from the E vs log Current Density graphs generated during cyclic polarization. Triplicate runs were performed.

Specimen from the three (3) samples were soaked in SBF for 0, 1, 3 and 7 days and the SEM micrographs taken. Additional exposure of the same specimen for extended time was not possible due to constraints in the return of the sample from the SEM EDS facility.

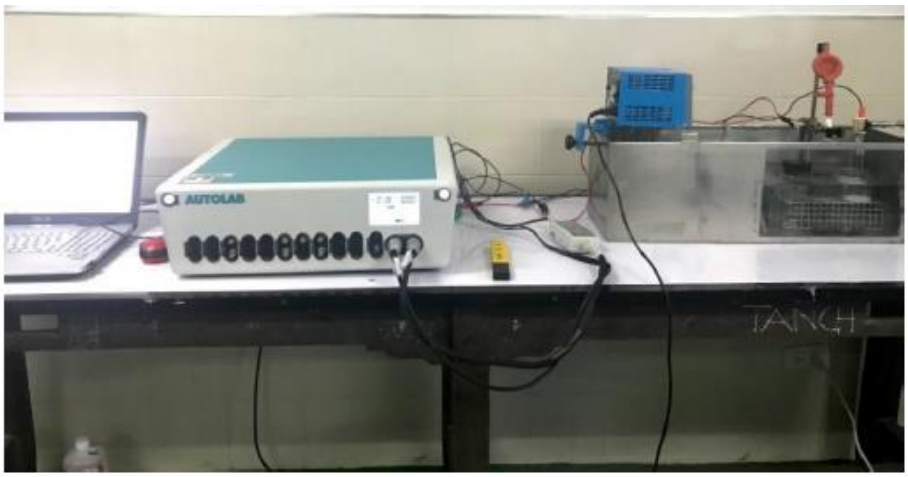

Figure 3. Electrochemical and Water Bath Set Up

IV. RESULTS AND DISCUSSION

4.1 Chemical Analyses by X-ray Fluorescence

Table 3 shows the chemical analyses of the samples using x-ray fluorescence spectroscopy. The technique, being a surface analysis method is unable to detect all of the components identified in Table 1, and may only be reliable for the major components iron, chromium and nickel. The results further show that Sample A appears to have a higher chromium contents when compared to Samples B and C.

4.2 Chemical Analysis by Spark Emission Spectroscopy

Spark Optical Emission Spectroscopy was performed to get a better compositional analysis of the samples and the results are summarized in Table 4. AISI ASTM Standard analyses are included for comparison.

The results show that Sample A is AISI 304 stainless steel while Samples B and C had compositions that corresponds to AISI 316L stainless steels. Visually, all the samples had the same appearance.

Table 3. XRF Analyses Results

%	Sample A	Sample B	Sample C
Iron	71.90	70.30	70.31
Nickel	8.32	10.69	10.59
Copper	0.19	0.69	0.79
Zinc	0.01	0.01	0.00
Tin	0.01	0.02	0.02
Lead	0.01	0.02	0.01
Chromium	17.68	15.81	15.81
Cobalt	0.15	0.22	0.23
Manganese	1.53	2.05	2.05
Tungsten	1.58	0.06	0.06
Vanadium	0.14	0.11	0.11

Table 4. Spark OES Results

%	Sample A	Sample B	Sample C	AISI 316L ASTM Standard	AISI 304 ASTM Standard
Carbon	0.081	0.028	0.032	0.03 max	0.08 max
Silicon	0.321	0.275	0.292	0.75 max	0.75 max
Manganese	0.891	1.473	1.410	2.00 max	2.00 max
Phosphorous	0.031	0.032	0.012	0.045 max	0.045 max
Sulfur	0.024	0.015	0.010	0.03 max	0.03 max
Chromium	17.637	15.923	15.947	16.00 - 18.00	18.00 - 20.00
Molybdenum	0.194	2.12	2.127	2.00 - 3.00	-
Nickel	8.12	10.08	9.977	10.00 - 14.00	8.00 - 12.00
Iron	Balance				

4.2 Cyclic Voltammetry Results

Cyclic voltammetry was performed to determine the susceptibility of the implants to pitting corrosion. The pitting potential, Epit and protection potential, Epro were determined using the E vs log current density graph. The size of the hysteresis loop, and the difference between Epro and Epit were used to evaluate the tendency towards pitting. A large hysteresis loop and a negative value of (Epro – Epit) indicate higher tendency towards pitting.

Figures 4, 5 and 6 show the polarization curves of the 3 samples after various times of immersion in the SBF. All samples displayed a hysteresis loop, although that for Sample A is larger than Samples B and C, thus indicating a higher pitting tendency. This could be expected since the OES analysis showed that Sample A is type SS304, and has a reported higher tendency towards pitting corrosion when compared to SS316L [13]. A similar study conducted by Sivakumar [14] of failed implants in India showed that the implant material is made from SS304. Samples B and C showed similar sizes of hysteresis loops. The number of soaking days does not appear to influence the tendency towards pitting. Pitting is observed even at zero days of soaking.

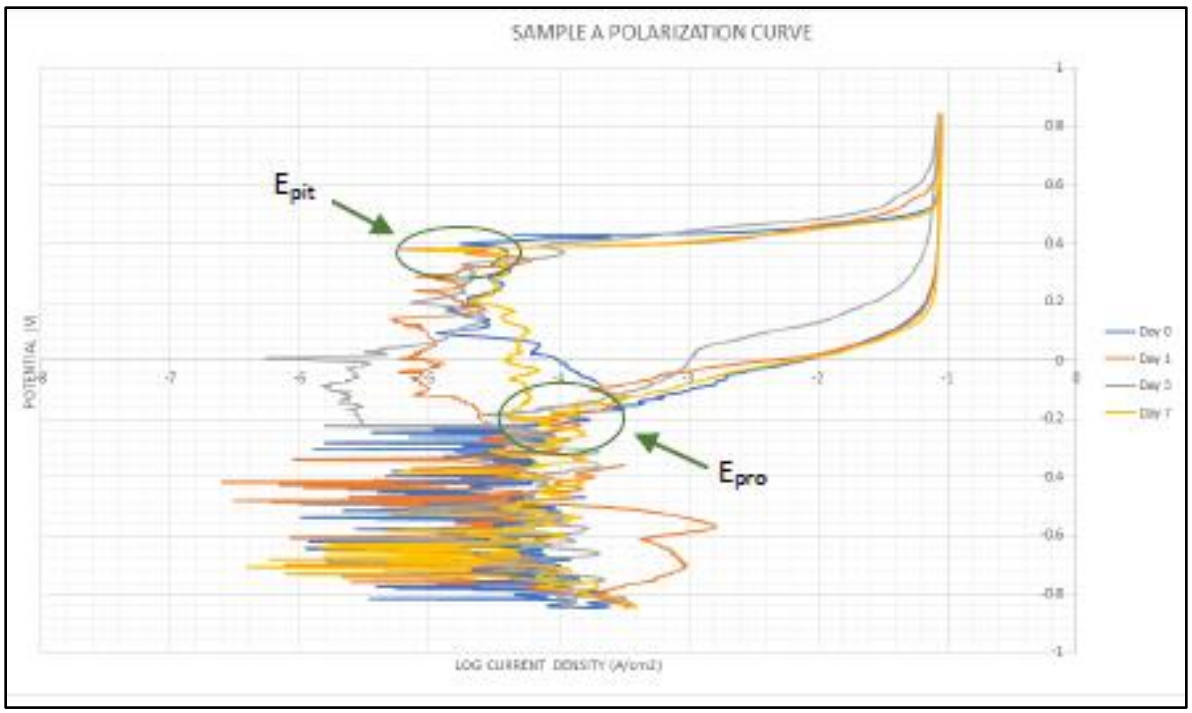

Figure 4. Cyclic Voltammetry Graphs for Sample A

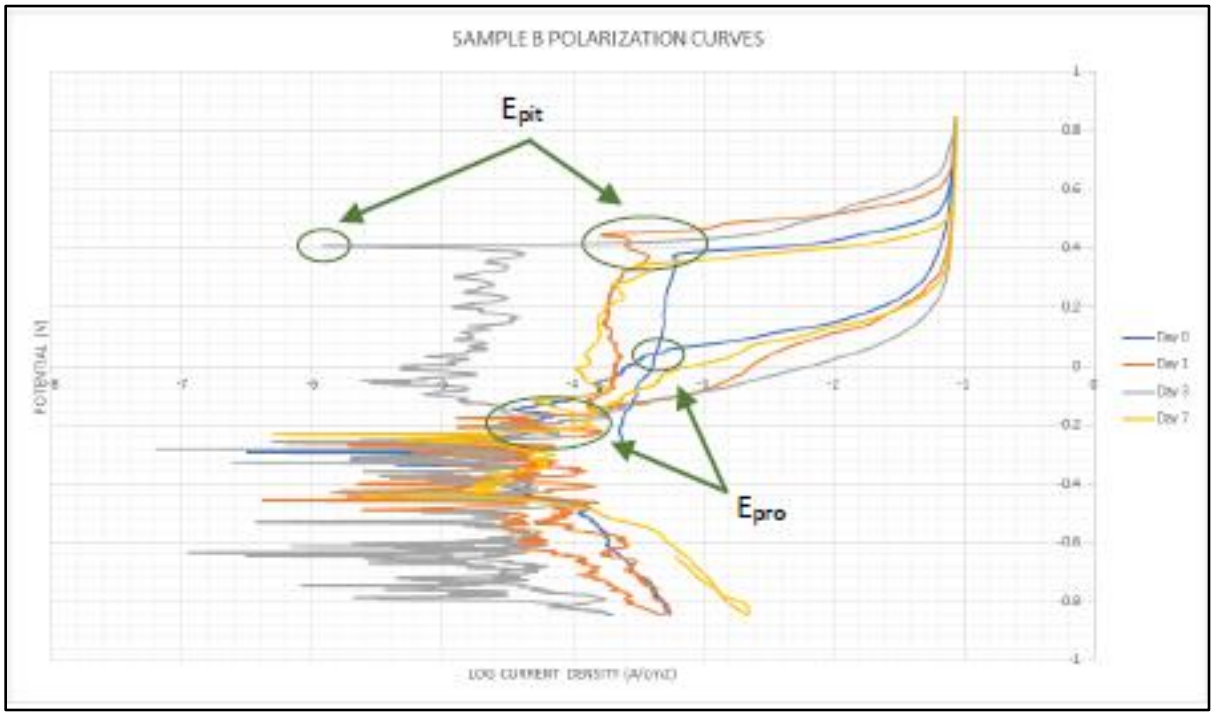

Figure 5. Cyclic Voltammetry Graphs for Sample B

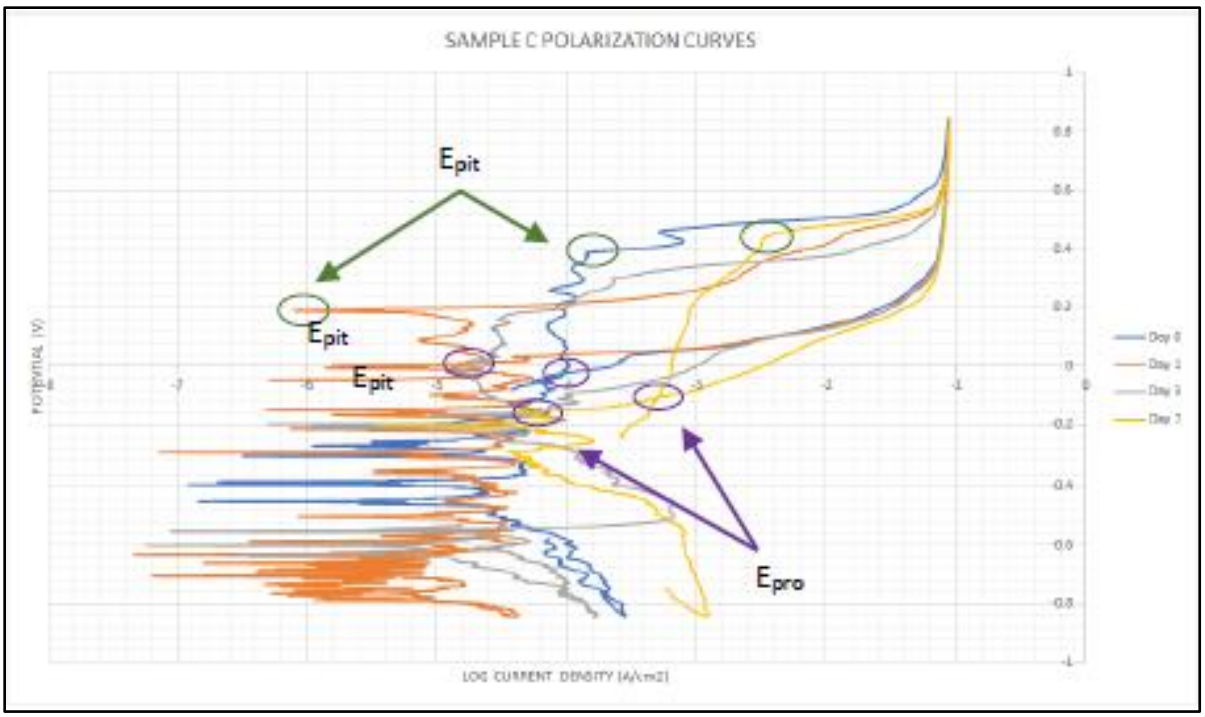

Figure 6. Cyclic Voltammetry Graph for Sample C

The values of (Epro – Epit) for the various runs are summarized in Table 5. The results show that Sample A has the most negative (Epro – Epit) value, consistent with its largest hysteresis loop. Similarly, the number of soaking days does not appear to influence the tendency towards pitting for each sample.

Table 5. Summary of Epit and Epro Values

Sample A			
	Epit (V)	Epro (V)	Epro-Epit (V)
Day 0	0.429	-0.22	-0.649
Day 1	0.38	-0.274	-0.654
Day 3	0.388	-0.224	-0.612
Day 7	0.377	-0.197	-0.574
Sample B			
	Epit (V)	Epro (V)	Epro-Epit (V)
Day 0	0.366	0.042	-0.324
Day 1	0.441	-0.164	-0.605
Day 3	0.408	-0.2	-0.608
Day 7	0.34	-0.178	-0.518
Sample C			
	Epit (V)	Epro (V)	Epro-Epit (V)
Day 0	0.373	-0.029	-0.402
Day 1	0.19	0.017	-0.173
Day 3	0.289	-0.165	-0.454
Day 7	0.432	-0.114	-0.546

4.3 SEM-EDS Analysis

Representative specimen for each sample was subjected to SEM-EDS analysis. Figure 7 shows the amount of pitting for Sample A as a function of soaking time. These micrographs were taken from different specimen and as such could only be taken as an indication of the extent of corrosion. No quantification on the extent of corrosion is attempted. The number of pits increased as a function of soaking time, with less pits at Day 0 increasing towards Day 3. This may be due to the degradation of the initial passivation on the sample by the components upon continuous soaking in the SBF solution. Serious corrosion damage is observed at Day 7.

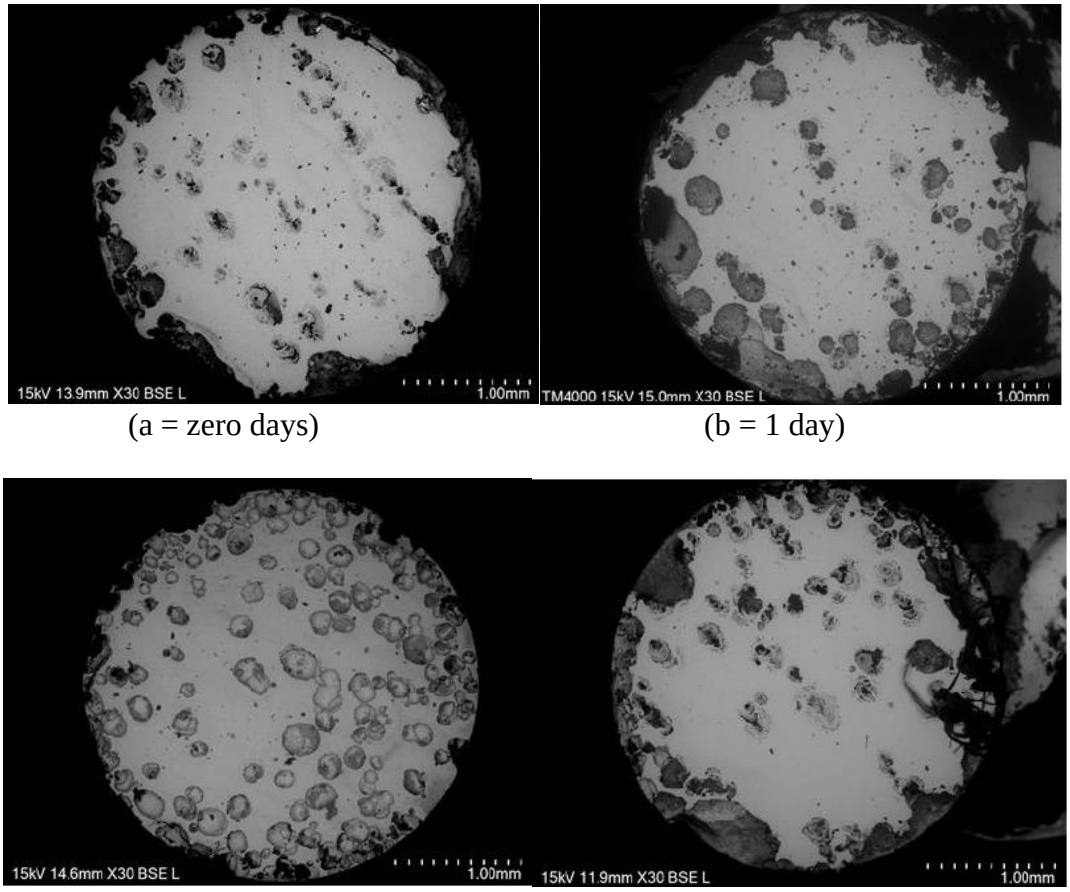

(a = zero days) (b = 1 day)

(c = 3 days) (d = 7 days)

Figure 7. SEM Micrographs of Sample A as a Function of Soaking Time

Figure 8 compares the amount of corrosion for the three (3) samples after 1 day of soaking. The extent of pitting corrosion is observed to be higher in Sample A when compared to Samples B and C. In these micrographs, Samples B and C appear to have the same level of corrosion damage.

EDS mapping of the corroded surface showed the presence of oxides and chlorides in the pit area, as shown in Figure 9. During the dissolution of iron, electrons are given up by the oxidation reaction:

$$Fe \rightarrow Fe^{2+} + 2e^{-} \quad \text{(Eq. 1)}$$

These electrons flow to the cathodic area where they are consumed by the following reaction:

$$1/2O_2 + H_2O + 2e^{-} \rightarrow 2(OH)^{-} \quad \text{(Eq. 2)}$$

Further, the ions released in the anodic dissolution of iron causes the electrolyte inside the pit to be positively charged, thus attracting more chloride ions. These chloride ions react with ferrous ions and precipitated ferrous chloride. Ferrous chloride, in equilibrium with water generated hydrochloric acid according to Eqn 4, further accelerating the corrosion process [15]. This results into the autocatalytic corrosion of stainless steel. Ferrous hydroxide is also precipitated during the reaction. The large cathode and small anode combination also favors the increase in the rate of corrosion and the penetration depth of the pit.

$$Fe^{2+} + 2Cl^{-} \rightarrow FeCl_2(s) \qquad \text{(Eqn 3)}$$

$$FeCl_2(s) + 2H_2O \rightarrow Fe(OH)_2(s) + 2HCl \qquad \text{(Eqn 4)}$$

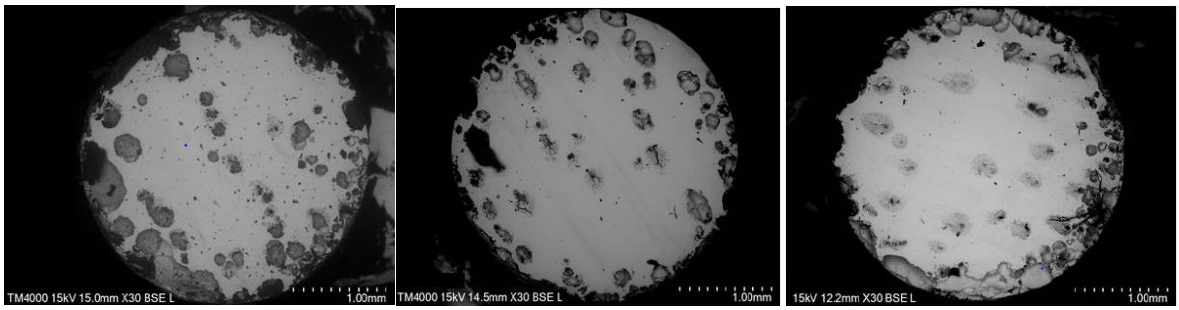

(Sample A) (Sample B) (Sample C)

Figure 8. SEM Micrograph of Samples A, B and C after 1 Days Soaking

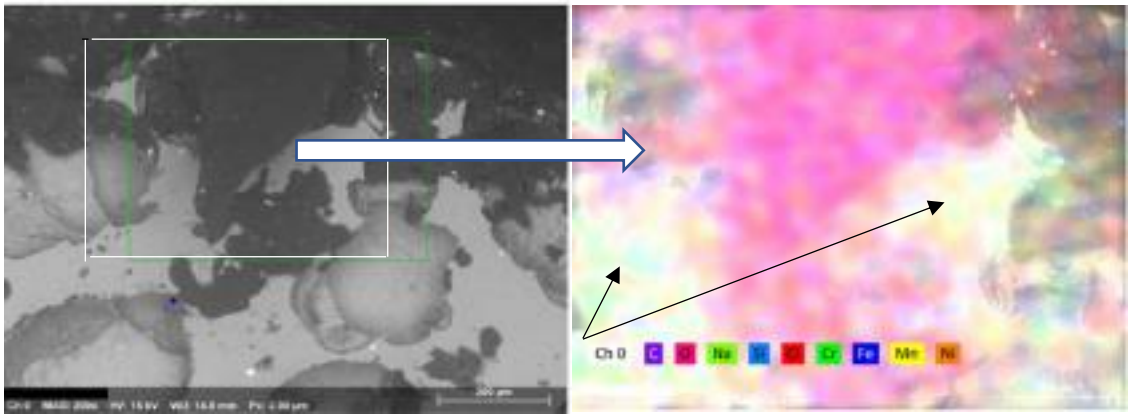

Figure 9. SEM Micrographs and EDS Map of Sample A (Day 3 Soak) Showing Chlorine and Oxygen in the Pit Area

V. CONCLUSIONS

The study demonstrates the susceptibility of locally available Steinmann pins to pitting corrosion in Kokubo simulated body fluid solution. The pitting corrosion starts immediately and proceeds autocatalytically. Optical Emission Spark Spectroscopic analysis showed that both SS304 and SS316L are being sold locally as Steinmann pins. SS304 steel is shown to be more susceptible to pitting corrosion in comparison with SS316L.

VI. RECOMMENDATION

The failure analysis of Steinmann pins retrieved from patients would be a good follow on to this work. This should be correlated with the length of time the implant has been in place. Analysis of sepsis or infection of surrounding tissues with respect to ionic contamination will provide insights on the deleterious component of the stainless steel. Performance in comparison with TiAlV alloys and apatite passivated implants may also be performed.

REFERENCES

[1] Saldana, E., "2015 POC Census", Quezon City (private communication)

[2] Chew, K. K., et al, "The Corrosion Schenario in human body: Stainless Steel 316L Orthopeadic Implants", **Natural Science**, Vol. 4, No. 3, 184-188, **2012**.

[3] Mcguire, M. F., Stainless Steels for Design Engineers, ASM International, 2008.

[4] Kokubo, T., "Bioactive Glass Ceramics:Preparations, Properties and Applications", **Biomaterials**, Vol. 12, 155-163, **1991**.

[5] Kokubo, T., and Takadama, H., "How Useful is SBF in Predicting in vivo bone Bioactivity", **Biomaterials**, Vol. 27, 2907-2015, **2006**.

[6] Hansen, D., "Metal Corrosion in the Human Body: The Ultimate Bio-Corrosion Scenario", **Electrochemical Society Interface**, Vol. 17, 31-34, **2008**.

[7] Mohd, T. et al, "Potentiodynamic Polarization Study of Type 316L and 316LVM Stainless Steels for Surgical Implants in Simulated Body Fluid", **Journal of Chemical and Pharmaceutical Research**, 203-208, 2**012**.

[8] Yang, H., et al., "Pitting Corrosion Resistance of La added 316L Stainless Steel in Simulated Body Fluids", Materials Letters Science **Direct**, Vol. 61, 1154-1157, 2007.

[9] Esmailzadeh, S, et. al., "Interpretation of Cyclic Potentiodaynamic Polarization Test Results for the Study of Corrosion Behavior of Metals: A Review", **Protection of Metals and Physical Chemistry of Surfaces**, Vol. 54, No. 5, 976-989, **2018**.

[10] Mena, M. G. Lectures in Special Topics in Electrometallurgy, Chapter 8, Experimental Techniques, Met E 298.

[11] Kamran, M., et. al., "Investigating the Pitting Resistance of 316 Stainless Steel in Ringer's Solution using the Cyclic Polarization Technique", Defect and Diffusion Forum, Vol. 334, 1 – 1. **2013**.

[12] Princeton Applied Research, Application Note CORR-1, Basics of Corrosion Measurement, www.princetonappliedresearch.com

[13] Shakir, I., et. al., "Pitting Corrosion Behavior of 304SS and 316SS Alloys in Aqueous Chloride and Bromide Solutions", **Journal of Engineering**, Vol. 24, No. 1, 53-69, **2018**.

[14] Sivakumar, M., and Rajeswari, S., "Investigation of Failures in Stainless Steel Orthopeadic Implant Devices: Pit-Induces Stress Corrosion Cracking", **Journal of Materials Science Lectures**, Vol. 11, 1039-1042, **1992**.

[15] Ma, FY, "Corrosive Effects of Chlorides on Metals", **Pitting Corrosion**, Bensalah, N. (ed), ISBN: 978-953-51-0275-5, Intech, www.intechopen.com, **2012**.